Acta Mech 227, 2831–2842 (2016)
DOI 10.1007/s00707-016-1651-0

ORIGINAL PAPER

Yu. Vetyukov · P. G. Gruber · M. Krommer

Nonlinear model of an axially moving plate in a mixed Eulerian–Lagrangian framework

Received: 28 November 2015 / Revised: 15 April 2016 / Published online: 21 May 2016

Abstract We consider finite deformations and bending of an elastic plate moving across a given domain. Velocities of the plate are kinematically prescribed at two parallel lines, which bound the region in the direction of motion. Inhomogeneity of the velocity profile at the exit from the domain results in planar deformations and out-of-plane buckling of the plate. The presented quasistatic analysis features a novel kinematic description, in which the coordinate in the direction of motion is a Eulerian one, while the displacements in transverse and the out-of-plane directions are modeled in a Lagrangian framework. The material volume is traveling across a finite element mesh, which is aligned to the boundaries of the domain. A concise mathematical formulation results in a robust numerical scheme without the need to solve the advection (transport) equation at each time step. The model is validated against solutions of a benchmark problem with a conventional Lagrangian finite element scheme. The approach is further demonstrated by modeling the time evolution of deformation of a moving plate.

1 Introduction

A vast body of literature is devoted to modeling dynamics and deformations of axially moving strings, beams or plates, see a review paper by Chen [2]. The material particles are continuously entering and leaving the considered region, which makes the analysis with the conventional Lagrangian (material) description difficult and inefficient. Eulerian description helps restricting the attention to the domain of interest and provides a possibility to apply the boundary conditions at spatially fixed points. Transforming the equations of motion of the structure to the spatial frame is particularly challenging in a geometrically nonlinear setting, especially when the gross axial motion is not prescribed in advance, but rather needs to be determined as a part of the solution, see Humer and Irschik [3], Eliseev and Vetyukov [4], Pechstein and Gerstmayr [5] for one-dimensional structures such as beams and strings. Care needs to be taken when the equations for an open system are derived directly "from scratch" using variational principles, see Irschik and Holl [6].

Previous attempts to obtain a model for an axially moving deformable plate [7,8] did not account for particular kinematic conditions at the boundaries of the domain in the form of time and space variations of the prescribed velocity profiles. These effects are particularly relevant in applications of hot rolling, strip coiling or belt drive simulations.

First account of these results has been presented by the authors at the Mini-Symposium "Axially Moving Structures" at PCM-CMM-2015 Conference in Gdansk, see [1].

Yu. Vetyukov (✉) · M. Krommer
Vienna University of Technology, Getreidemarkt 9, 1060 Vienna, Austria
E-mail: yury.vetyukov@tuwien.ac.at

P. G. Gruber
Linz Center of Mechatronics, Altenbergerstraße 69, 4040 Linz, Austria

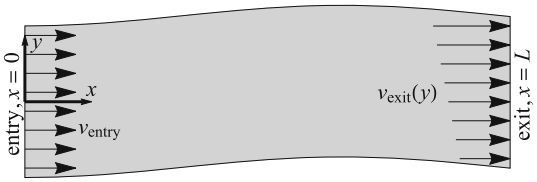

Fig. 1 Deformable plate moving in the axial direction (x) with kinematically prescribed velocities; the velocity profile at the exit from the domain is varying in the transverse direction (y)

In this paper we present a novel mathematical description for finite deformations of a thin plate, which is moving between two parallel lines, see Fig. 1. This gross axial motion takes place in the direction of the x-axis (called in the following axial direction) from left to right. Velocities of the plate at the entry to the domain $x = 0$ and at the exit from it $x = L$ are kinematically prescribed and equal respectively v_{entry} and v_{exit}. In a transient process, a non-constant profile of the velocity $v_{\text{exit}}(y)$ results in the deformation of the plate in its plane xy and subsequent buckling in the out-of-plane direction of the z-axis. This kind of undesired behavior may happen during the metal rolling process, paper production, etc., which makes the respective methods of analysis practically relevant.

The proposed Eulerian-Lagrangian formulation is motivated by computational difficulties that are inherent in conventional finite element modeling of the deformation of the plate. As a Lagrangian finite element mesh propagates across the domain in the course of a simulation, kinematic boundary conditions need to be imposed at the interior of the finite elements. This typical "variational crime" leads to numerically induced oscillatory behavior of the stressed state of the plate, and this would not allow for accurate presentation of its bending, which is tightly coupled with the in-plane stresses. While extended finite element formulations [9] or a mortar approach [10] could theoretically be applied to solving the issue, an elegant and efficient alternative is to preserve the finite element mesh from moving in the axial direction. This guarantees that the boundaries of the active domain, at which the displacements need to be prescribed for each time step, remain aligned with the boundaries of the finite element mesh.

The newly proposed idea of transformation of the nonlinear equations of the plate theory to another set of coordinates resembles the known Arbitrary Lagrangian-Eulerian (ALE) formulation, which often finds use for simulations of the process of material production and forming [11–13]. Considering x as an Eulerian coordinate and using a material description for the transverse and out-of-plane displacements, we achieve a clear and robust numerical scheme. The mathematical transformations become particularly simple with the use of the direct tensor calculus. At each time step, the mechanical equilibrium is sought directly in the mixed description. We thus avoid the need of separating the time step into a Lagrangian phase, followed by the mesh update and remapping of the nodal entities onto the new mesh using the model of advection, which is intrinsic to ALE. To the best knowledge of the authors, this is a first open literature presentation of a fully nonlinear plate model at non-material description.

The Kirchhoff-Love geometrically nonlinear theory of unshearable plates was put into the basis of the presented analysis and simulations, see [14–17]. This classical model shall be accurate enough for the considered thin structures, and the applied finite element scheme [18] benefits from the absence of shear locking. Nevertheless, the transformation of the theory to a mixed Eulerian-Lagrangian set of coordinates shall be equally feasible for a shear deformable Reissner-Mindlin type model with independent translations and rotations of particles [19].

At present, we restrict the consideration to the constant profile of the velocity of material production v_{entry} and aim at modeling the evolution of finite deformations of an elastic plate under quasistatic assumptions. Further extensions of the approach are discussed in the concluding remarks below.

2 Kinematic description

Consider a plate as a two-dimensional material surface axially moving across a domain, bounded by two lines, see Fig. 2. Rolling of a sheet of metal, paper production or motion of a conveyor belt are typical examples of such a structure. At each time instant, the plate is clamped at the lines of contact: there are no out-of-plane displacements in the direction of the z axis at $x = 0$ and $x = L$ nor does the plate rotate about these lines. The material is produced in a fixed segment $-w/2 \le y \le w/2$ at $x = 0$, such that the plate is here centered

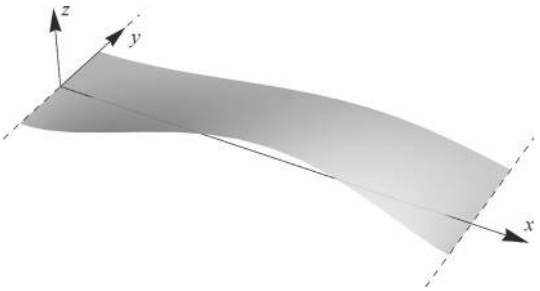

Fig. 2 Deformable plate, moving across a domain, bounded by two lines (*dashed*): three-dimensional view

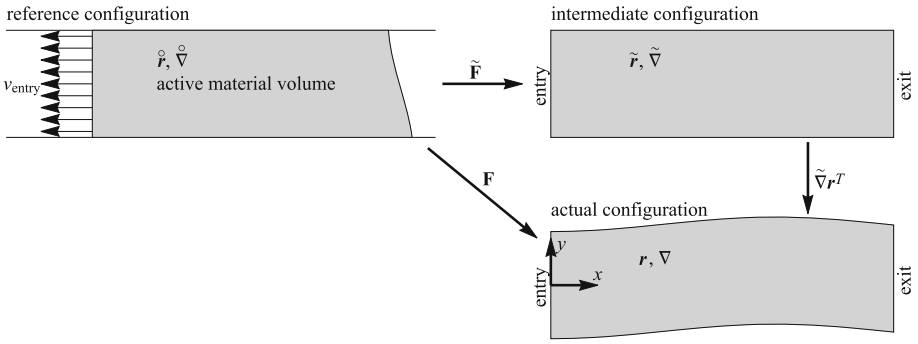

Fig. 3 Configurations involved in the mathematical description of the kinematics of the plate

and has a fixed width w. The second line of contact, where the plate is leaving the domain, may travel in the transverse direction, see the discussion in Sect. 6.

For the sake of mathematical description, we introduce an infinitely long *reference configuration*, see Fig. 3. Particles of the plate are identified by their material coordinates $\mathring{x}$ and $\mathring{y}$, i.e., by the reference position vector

$$\mathring{\boldsymbol{r}} = \mathring{x}\boldsymbol{i} + \mathring{y}\boldsymbol{j}, \quad -w/2 \le \mathring{y} \le w/2 \tag{1}$$

with $\boldsymbol{i}$, $\boldsymbol{j}$, and $\boldsymbol{k}$ being the unit base vectors of the global Cartesian frame. In the *actual state*, we consider just the particles, which are currently residing in the domain $0 \le x \le L$. In the reference configuration these particles form a planar manifold, which will be called *active material volume* in the following (depicted gray in Fig. 3), and which is thus a pre-image of the actual state. Between the time instants t and $t + \mathrm{d}t$, a material layer of the length $v_{\text{entry}}\,\mathrm{d}t$ enters the domain from the left. As $v_{\text{entry}} = \text{const}$, it means that the left boundary of the active material volume (which is a pre-image of the line $x = 0$, $-w/2 \le y \le w/2$ in the actual configuration) is moving across the stress free reference configuration to the left with the velocity v_{entry}, the mathematical form of this statement being (41).

The Lagrangian description, at which the actual configuration is defined by a mapping from $\mathring{\boldsymbol{r}}$ to the actual place of a particle

$$\boldsymbol{r} = x\boldsymbol{i} + y\boldsymbol{j} + z\boldsymbol{k}, \tag{2}$$

remains efficient as long as the active material volume is known (and suitable for being discretized in numerical simulations). This is not the case for the problem at hand, and it is efficient to decompose the mapping into two steps by introducing an additional spatially fixed *intermediate configuration*. This rectangular domain with the position vector

$$\tilde{\boldsymbol{r}} = \tilde{x}\boldsymbol{i} + \tilde{y}\boldsymbol{j}, \quad 0 \le \tilde{x} \le L, \quad -w/2 \le \tilde{y} \le w/2 \tag{3}$$

differs from the reference state by the axial displacement u_x only:

$$\tilde{\boldsymbol{r}} = \mathring{\boldsymbol{r}} + u_x\boldsymbol{i}, \quad \tilde{x} = \mathring{x} + u_x, \quad \tilde{y} = \mathring{y}. \tag{4}$$

At the same time, just the transverse displacement u_y and the out-of-plane displacement u_z differ the actual configuration from the intermediate one:

$$\boldsymbol{r} = \tilde{\boldsymbol{r}} + u_y\boldsymbol{j} + u_z\boldsymbol{k}, \quad x = \tilde{x}, \quad y = \tilde{y} + u_y, \quad z = u_z. \tag{5}$$

Now, as

$$\tilde{x} = x, \quad \tilde{y} = \mathring{y}, \tag{6}$$

the left and the right boundaries of the intermediate configuration (3) map onto the lines of contact of the plate $x = 0$ and $x = L$. We thus introduce the mapping from the active material volume in the reference configuration to the actual state implicitly in the form

$$\mathring{\boldsymbol{r}} = \mathring{\boldsymbol{r}}(\tilde{\boldsymbol{r}}), \quad \boldsymbol{r} = \boldsymbol{r}(\tilde{\boldsymbol{r}}), \tag{7}$$

which guarantees the conformity of the domains.

3 Deformation and strain energy

Treating displacements

$$\boldsymbol{u} = u_x \boldsymbol{i} + u_y \boldsymbol{j} + u_z \boldsymbol{k} \tag{8}$$

as primary variables, we seek them as functions of the place in the intermediate configuration:

$$\boldsymbol{u} = \boldsymbol{u}(\tilde{\boldsymbol{r}}) = \boldsymbol{r} - \mathring{\boldsymbol{r}}. \tag{9}$$

The quasistatic simulations below are based on the principle of stationarity of the total strain energy of the active volume of the plate at each time instance. For a classical (unshearable) Kirchhoff plate model, the energy depends on the two Green–Lagrange-type strain measures, which are referred to the change of the in-plane metric of the plate and to its curvature [14,15]. It appears to be convenient to employ the modern formulation of the theory [16,17,20] with the symmetric *strain tensors*

$$\begin{aligned} \mathbf{E} &= \frac{1}{2}(\mathbf{F}^T \cdot \mathbf{F} - \mathbf{I}_2), \\ \mathbf{K} &= \mathbf{F}^T \cdot \mathbf{b} \cdot \mathbf{F}. \end{aligned} \tag{10}$$

The first strain measure $\mathbf{E}$ describes the membrane (in-plane) deformation of the plate, while the second one $\mathbf{K}$ is responsible for its bending. The *gradient of deformation* is the transposed gradient of the position vector of the actual state with respect to the reference one:

$$\begin{aligned} \mathbf{F} &= \mathring{\nabla} \boldsymbol{r}^T, \\ \mathring{\nabla} &= \boldsymbol{i} \frac{\partial}{\partial \mathring{x}} + \boldsymbol{j} \frac{\partial}{\partial \mathring{y}} \equiv \boldsymbol{i}\, \partial_{\mathring{x}} + \boldsymbol{j}\, \partial_{\mathring{y}}. \end{aligned} \tag{11}$$

The in-plane *identity tensor* is

$$\mathbf{I}_2 = \boldsymbol{i}\boldsymbol{i} + \boldsymbol{j}\boldsymbol{j} = \mathring{\nabla} \mathring{\boldsymbol{r}}, \tag{12}$$

and the second metric tensor of the actual configuration

$$\mathbf{b} = -\nabla \boldsymbol{n} \tag{13}$$

is the negative gradient of the *unit normal vector* $\boldsymbol{n}$ to the actual surface of the plate [14,21]. We recall the relation between the differential operators of the reference and of the actual states,

$$\mathring{\nabla} = \mathbf{F}^T \cdot \nabla, \tag{14}$$

and rewrite the second equality in (10):

$$\mathbf{K} = -\mathring{\nabla} \boldsymbol{n} \cdot \mathbf{F}. \tag{15}$$

Now, the displacement (9) is a field over the intermediate configuration, which does not allow us to directly compute the strain tensors using (10). We aim at *transforming the above kinematic relations* from the material

description featuring derivatives with respect to the coordinates in the reference state *to the differential operator of the intermediate configuration*

$$\tilde{\nabla} = \boldsymbol{i}\,\partial_{\tilde{x}} + \boldsymbol{j}\,\partial_{\tilde{y}}. \tag{16}$$

For a two-stage mapping from the reference configuration to the actual one, the total deformation gradient is a product

$$\mathbf{F} = \tilde{\nabla}\boldsymbol{r}^T \cdot \mathring{\tilde{\nabla}}\tilde{\boldsymbol{r}}^T, \tag{17}$$

which is mathematically equivalent to the chain rule of differentiation of a function of multiple arguments. We introduce the gradient of deformation from the reference configuration to the intermediate one

$$\tilde{\mathbf{F}} = \mathring{\tilde{\nabla}}\tilde{\boldsymbol{r}}^T = \left(\mathbf{I}_2 - \boldsymbol{i}\,\tilde{\nabla}u_x\right)^{-1}. \tag{18}$$

Indeed, using a relation between the differential operators analogous to (14) and recalling (4), we write

$$\begin{aligned} &\mathring{\nabla} = \tilde{\mathbf{F}}^T \cdot \tilde{\nabla}, \\ &\mathbf{I}_2 = \mathring{\nabla}\mathring{\boldsymbol{r}} = \tilde{\mathbf{F}}^T \cdot \tilde{\nabla}\,(\tilde{\boldsymbol{r}} - u_x\boldsymbol{i}) = \tilde{\mathbf{F}}^T \cdot \left(\mathbf{I}_2 - \tilde{\nabla}u_x\boldsymbol{i}\right) \quad \Rightarrow \quad (18). \end{aligned} \tag{19}$$

The inverse of an in-plane tensor in (18) is again an in-plane one, and the total deformation gradient $\mathbf{F}$ can now be computed for any field of displacements (9), known in the intermediate configuration (3).

While this is sufficient for the membrane strains $\mathbf{E}$ in (10), further mathematics is needed to compute the tensor of bending strains $\mathbf{K}$. Using the first relation in (19), we rewrite (15) as

$$\mathbf{K} = \tilde{\mathbf{F}}^T \cdot \tilde{\mathbf{K}} \cdot \tilde{\mathbf{F}}, \tag{20}$$

in which a symmetric tensor

$$\tilde{\mathbf{K}} = -\tilde{\nabla}\boldsymbol{n} \cdot \tilde{\nabla}\boldsymbol{r}^T \tag{21}$$

is introduced.

The vector of unit normal is easy to compute with the known relation $\boldsymbol{r}(\tilde{\boldsymbol{r}}) = \boldsymbol{r}(\tilde{x}\boldsymbol{i} + \tilde{y}\boldsymbol{j})$. Considering a surface, parametrized by coordinates x and $\tilde{y}$, we write

$$\boldsymbol{n} = \frac{\partial_{\tilde{x}}\boldsymbol{r} \times \partial_{\tilde{y}}\boldsymbol{r}}{|\partial_{\tilde{x}}\boldsymbol{r} \times \partial_{\tilde{y}}\boldsymbol{r}|}. \tag{22}$$

From (5) we see that $\boldsymbol{n}$ at a given point of the intermediate configuration does not depend on the field $u_x(\tilde{\boldsymbol{r}})$. Now we apply $\tilde{\nabla}$ to both sides of the identity

$$\tilde{\nabla}\boldsymbol{r} \cdot \boldsymbol{n} = \left(\boldsymbol{i}\,\partial_{\tilde{x}}\boldsymbol{r} + \boldsymbol{j}\,\partial_{\tilde{y}}\boldsymbol{r}\right) \cdot \boldsymbol{n} = 0 \tag{23}$$

and arrive at an alternative form of (21), which makes the symmetry of $\tilde{\mathbf{K}}$ better visible:

$$\tilde{\nabla}\tilde{\nabla}\boldsymbol{r} \cdot \boldsymbol{n} = -\tilde{\nabla}\boldsymbol{n} \cdot \tilde{\nabla}\boldsymbol{r}^T = \tilde{\mathbf{K}}. \tag{24}$$

The above general nonlinear kinematic relations may be simplified when particular deformations or coupling terms are negligible. Thus, in a *geometrically linear model* just small deformations are assumed to be superposed upon a regular axial motion of the plate, and linearizing we arrive at the conventional strains of the classical plate theory:

$$\mathbf{E} \approx \boldsymbol{\varepsilon} = \nabla(u_x\boldsymbol{i} + u_y\boldsymbol{j})^S, \quad \mathbf{K} \approx \boldsymbol{\kappa} = \nabla\nabla u_z. \tag{25}$$

In a linear theory, one does not need to differentiate between ∇ and $\tilde{\nabla}$, and conventional finite element models of a plate may be applied. However, in this linear formulation, the in-plane stresses are decoupled from the bending of the plate, which makes it inapplicable for studying buckling behavior.

Returning to the fully nonlinear model, we write the strain energy of a plate per unit area of its reference configuration as a quadratic form of the strains [17]:

$$U = \frac{1}{2}\left(A_1(\mathrm{tr}\mathbf{E})^2 + A_2\mathbf{E}\cdot\cdot\mathbf{E} + D_1(\mathrm{tr}\mathbf{K})^2 + D_2\mathbf{K}\cdot\cdot\mathbf{K}\right). \tag{26}$$

Thus, we assume that the local strains remain small, which does not exclude large overall deformations of a thin structure. For a homogeneous isotropic plate with the thickness h, Young's modulus E, and Poisson's ratio ν, the stiffness coefficients are

$$A_1 = \frac{E\nu h}{1-\nu^2}, \quad A_2 = \frac{Eh}{1+\nu}, \quad D_1 = \frac{h^2}{12}A_1, \quad D_2 = \frac{h^2}{12}A_2. \tag{27}$$

Now, we need to integrate the strain energy over the intermediate configuration. The change of variables is to be accounted for,

$$\mathrm{d}\mathring{x}\,\mathrm{d}\mathring{y} = (\det\tilde{\mathbf{F}})^{-1}\,\mathrm{d}\tilde{x}\,\mathrm{d}\tilde{y}, \tag{28}$$

with

$$(\det\tilde{\mathbf{F}})^{-1} = 1 - \partial_{\tilde{x}}u_x, \tag{29}$$

see (18). Finally, the total strain energy of the active material volume reads

$$U_\Sigma = \int_0^L \mathrm{d}\tilde{x}\int_{-w/2}^{w/2}(1-\partial_{\tilde{x}}u_x)\,U\,\mathrm{d}\tilde{y}. \tag{30}$$

In the absence of external loading, U_Σ will be at minimum in a state of stable static equilibrium provided that the set of material particles is fixed. Although we are dealing with an open system, and particles are continuously entering and leaving the active material volume, this condition is fulfilled at each time step of a quasistatic simulation owing to the kinematic nature of the boundary conditions at both ends of the domain, see the discussion in Sect. 6 below.

4 Finite element scheme

In a numerical scheme, we need to compute the total strain energy U_Σ and its derivatives for a given approximation of displacements $\boldsymbol{u}(\tilde{\boldsymbol{r}})$. We have applied a four-node C^1-continuous finite element approximation, which is based on the idea of a Bogner-Fox-Schmit rectangle with bi-cubic shape functions, see [18,20]. A regular mesh was introduced in the intermediate configuration with $n_x \times n_y$ elements in the axial direction and in the transverse one, respectively. With twelve degrees of freedom at each node (vector of displacement, its two derivatives with respect to the local coordinates on the element, and one mixed second-order derivative), we guarantee the continuity of both $\boldsymbol{u}$ and $\boldsymbol{n}$ across the boundaries of the element. Now, the first strain measure $\mathbf{E}$ is continuous, and the second one $\mathbf{K}$ may undergo discontinuities of the first kind, which is sufficient for the regularity of the integral (30).

At each time instant, we fix the values of displacements at the boundaries $x = 0$ and $x = L$ according to (45). Along with the condition of clamping $\boldsymbol{n} = \boldsymbol{k}$, this results in kinematic constraints for some of the degrees of freedom. Seeking for a stable equilibrium, we minimize U_Σ with respect to the remaining degrees of freedom of the model e with the help of a quasi-Newton scheme, which requires computing derivatives of the kind

$$\frac{\partial U_\Sigma}{\partial e} = \int_0^L \mathrm{d}\tilde{x}\int_{-w/2}^{w/2}\left((1-\partial_{\tilde{x}}u_x)\,\frac{\partial U}{\partial e} - \frac{\partial(\partial_{\tilde{x}}u_x)}{\partial e}U\right)\mathrm{d}\tilde{y}. \tag{31}$$

A Gaussian integration rule with 3×3 points per element is used, and at each integration point we compute

$$\frac{\partial U}{\partial e} = (A_1\mathbf{I}_2\mathrm{tr}\mathbf{E} + A_2\mathbf{E})\cdot\cdot\frac{\partial\mathbf{E}}{\partial e} + (D_1\mathbf{I}_2\mathrm{tr}\mathbf{E} + D_2\mathbf{E})\cdot\cdot\frac{\partial\mathbf{K}}{\partial e}. \tag{32}$$

The difficulty lies at evaluating the derivatives of the strain measures with respect to e. Writing

$$\frac{\partial\mathbf{E}}{\partial e} = \mathbf{F}^T\cdot\frac{\partial\mathbf{F}}{\partial e}, \quad \frac{\partial\mathbf{F}}{\partial e} = \frac{\partial\tilde{\nabla}\boldsymbol{r}^T}{\partial e}\cdot\tilde{\mathbf{F}} + \tilde{\nabla}\boldsymbol{r}^T\cdot\frac{\partial\tilde{\mathbf{F}}}{\partial e}, \tag{33}$$

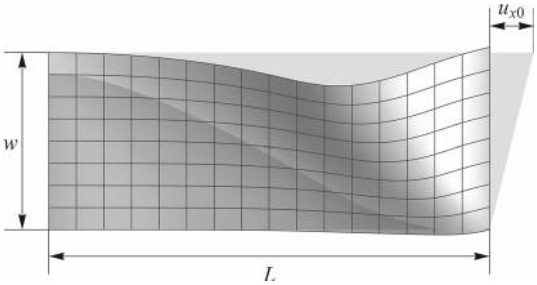

Fig. 4 Undeformed geometry of a trapezoidal plate and its supercritical configuration after the inclined edge is kinematically rotated

we see that either the first or the second term remain in the last expression depending on the kind of the degree of freedom at hand. Indeed,

$$\frac{\partial \tilde{\nabla} \boldsymbol{r}^T}{\partial e} = \left(\tilde{\nabla} \frac{\partial (u_y \boldsymbol{j} + u_z \boldsymbol{k})}{\partial e} \right)^T, \tag{34}$$

which vanishes if e is a degree of freedom of axial motion. Considering now the second term in (32), we write

$$\frac{\partial \mathbf{K}}{\partial e} = \tilde{\mathbf{F}}^T \cdot \frac{\partial \tilde{\mathbf{K}}}{\partial e} \cdot \tilde{\mathbf{F}} + 2\tilde{\mathbf{F}}^T \cdot \tilde{\mathbf{K}} \cdot \frac{\partial \tilde{\mathbf{F}}}{\partial e}. \tag{35}$$

Again, either the first or the second term needs to be treated depending on the kind of e.

Although programming the computation according to (32)-(35) is feasible, it would be a challenging task to obtain the second-order derivatives in an algorithmic manner. In the present study, we used a system of computer algebra *Wolfram Mathematica*[1] and first computed the first- and the second-order derivatives of the strain measures with respect to the local geometric characteristics

$$\partial_{\tilde{x}} \boldsymbol{u}, \quad \partial_{\tilde{y}} \boldsymbol{u}, \quad \partial^2_{\tilde{x}} \boldsymbol{u}, \quad \partial^2_{\tilde{y}} \boldsymbol{u}, \quad \partial_{\tilde{x}} \partial_{\tilde{y}} \boldsymbol{u}. \tag{36}$$

The resulting expressions were exported as automatically generated `C#` code into the in-house finite element simulation software. Now, the derivatives of (36) with respect to the nodal degrees of freedom are just the shape functions of a finite element, and the element's stiffness matrix and force vector are easily computed using the chain rule.

5 Benchmark problem

The kinematic formulation and the resulting finite element scheme were validated on a simple benchmark problem. Consider a plate of a trapezoidal shape. The width of the plate is w, while the other two edges have lengths L and $L + u_{x0}$ as in Fig. 4. The right (inclined) edge is clamped and kinematically rotated such that it becomes parallel to the left one, which is also clamped. Depending on the magnitude of u_{x0}, the resulting deformation of the plate in its own plane may become unstable and lead to the out-of-plane buckling as depicted in the figure by the surface with the grid lines on it.

As the deformed configuration is bounded between two parallel lines, the problem is perfectly suitable for the mixed Eulerian-Lagrangian description. At the same time, a solution with the conventional Lagrangian finite elements with the same approximation [18] is readily available, which allows comparing the solutions and thus testing the new numerical scheme.

Using SI system of units here and in the following, we summarize the parameters of the considered model:

$$L = 1, \quad w = 0.4, \quad u_{x0} = 0.1, \quad h = 5 \cdot 10^{-3}, \quad E = 2.1 \cdot 10^{11}, \quad \nu = 0.3. \tag{37}$$

Seeking for a static equilibrium, we considered an intermediate configuration $0 \le x \le L$, $-w/2 \le \tilde{y} \le w/2$ and prescribed u_x and u_y at the edge $x = L$ such that its pre-image in the reference state $\mathring{\boldsymbol{r}}$ would correspond to

[1] http://www.wolfram.com.

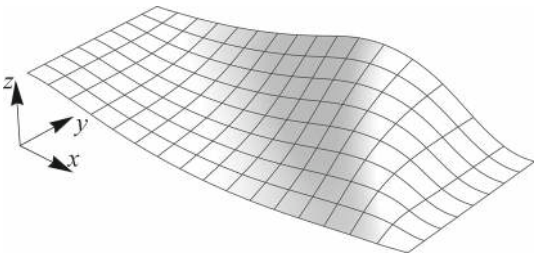

Fig. 5 Deformed configuration of a trapezoidal plate, kinematically loaded in its own plane

Table 1 Mesh convergence and comparison of the mixed Eulerian-Lagrangian and traditional Lagrangian frameworks for a benchmark problem

Discretization,	Mixed E.-L.		Lagrangian	
$n_x \times n_y$	$\min u_z$	$\max u_z$	$\min u_z$	$\max u_z$
4×2	-0.05851	0.18428	-0.07322	0.18138
8×4	-0.05546	0.18319	-0.05831	0.18256
16×8	-0.05496	0.18277	-0.05527	0.18259
32×16	-0.05493	0.18274	-0.05490	0.18262

the given undeformed geometry and the length of the rotated edge is preserved. The out-of-plane buckling was promoted by imposing a small gravity force in the first iteration of the quasi-Newton minimization scheme, which was then released for the rest of iterations.

In accordance with (5), the transverse grid lines of the finite element mesh, shown in the deformed state in Fig. 4 remain parallel to the y-axis. The surface of the plate in the supercritical state after buckling may be better observed from an isometric viewpoint as shown in Fig. 5. We studied the mesh convergence and compared the solutions with the proposed mixed Eulerian-Lagrangian description and with the conventional Lagrangian finite elements by finding the maximal and the minimal values of the displacement u_z, which are observed at the edges $\tilde{y} = \pm w/2$ of the plate. The results of the comparison, which are summarized in Table 1, clearly demonstrate that both formulations converge to the same solution.

6 Time stepping and boundary conditions

Time rates of mechanical entities need to be considered in a quasistatic simulation. We need to differentiate between the velocity of a particle $\dot{\boldsymbol{u}}$ with the *material time derivative*

$$(\cdots)^{\cdot} \equiv \left.\frac{\partial(\cdots)}{\partial t}\right|_{\mathring{\boldsymbol{r}}=\text{const}} \tag{38}$$

and the time rate $\partial_t \boldsymbol{u}$ with the *local derivative* at a given point in the intermediate configuration defined as

$$\partial_t(\cdots) \equiv \left.\frac{\partial(\cdots)}{\partial t}\right|_{\tilde{\boldsymbol{r}}=\text{const}}. \tag{39}$$

The general relation between the material and the local time derivatives with the known convective term reads

$$\dot{\boldsymbol{u}} = \frac{\mathrm{d}\boldsymbol{u}(\tilde{\boldsymbol{r}}(\mathring{\boldsymbol{r}}, t), t)}{\mathrm{d}t} = \partial_t \boldsymbol{u} + \dot{\tilde{\boldsymbol{r}}} \cdot \tilde{\nabla}\boldsymbol{u} = \partial_t \boldsymbol{u} + \dot{u}_x \boldsymbol{i} \cdot \tilde{\nabla}\boldsymbol{u} = \partial_t \boldsymbol{u} + \dot{u}_x\, \partial_{\tilde{x}} \boldsymbol{u}. \tag{40}$$

Observing the time evolution of nodal variables, we need to deal with the local time derivatives as the nodes of the finite element mesh are fixed in the intermediate configuration. As discussed after (1), the left boundary of the active material volume moves across the reference state with a known velocity, which means that the local time rate of $\boldsymbol{u}$ is known at the left edge:

$$x = 0: \quad \partial_t \mathring{\boldsymbol{r}} = -v_{\text{entry}} \boldsymbol{i} \quad \Rightarrow \quad \partial_t \boldsymbol{u} = v_{\text{entry}} \boldsymbol{i}. \tag{41}$$

On the opposite, at the right boundary, we know the actual velocities of the particles, with which they move across the line of contact:

$$x = L: \quad \dot{\boldsymbol{u}} = v_{\text{exit}}\boldsymbol{i}, \quad \dot{u}_x = v_{\text{exit}} \quad \Rightarrow \quad \partial_t \boldsymbol{u} = v_{\text{exit}}(\boldsymbol{i} - \partial_{\tilde{x}}\boldsymbol{u}). \tag{42}$$

This explains the fact that the right line of contact will move in the transverse direction as long as $\partial_{\tilde{x}}\boldsymbol{u}$ has a non-zero component in the direction of the y-axis (the z component is always zero owing to the condition of clamping). Indeed, in Fig. 1, the plate is slightly inclined immediately before $x = L$ and it is easy to imagine that in the next time instant a new cross-section of the plate with larger values of y will arrive at the line of contact. *Stationary motion* of the plate with

$$\boldsymbol{u} = \boldsymbol{u}_{\text{s}}(\tilde{\boldsymbol{r}}) + v_{\text{entry}} t\, \boldsymbol{i} \tag{43}$$

is possible only when the static deformation $\boldsymbol{u}_s$ fulfills

$$\begin{aligned} &x = 0: \quad \boldsymbol{u}_{\text{s}} = 0, \quad \boldsymbol{k} \cdot \partial_{\tilde{x}}\boldsymbol{u}_{\text{s}} = 0; \\ &x = L: \quad v_{\text{entry}}\boldsymbol{i} = v_{\text{exit}}(\boldsymbol{i} - \partial_{\tilde{x}}\boldsymbol{u}_{\text{s}}) \quad \Rightarrow \quad \partial_{\tilde{x}}\boldsymbol{u}_{\text{s}} = \left(1 - \frac{v_{\text{entry}}}{v_{\text{exit}}}\right)\boldsymbol{i}. \end{aligned} \tag{44}$$

These boundary conditions allow seeking the stationary solution by solving just a single static problem.

We turn back to the problem of evolution of the deformation of the plate in time. The strategy of computing the solution $\boldsymbol{u}^{(k+1)}$ in the end of a time step $t^{(k+1)} = (k+1)\tau$ for a known state of the plate $\boldsymbol{u}^{(k)}$ in the beginning of the time step $t^{(k)} = k\tau$ comprises the following two stages.

(i) First we compute new displacements at the left and right boundaries of the domain,

$$x = 0, L: \quad \boldsymbol{u}^{(k+1)} = \boldsymbol{u}^{(k)} + \tau\, \partial_t \boldsymbol{u}, \tag{45}$$

in which the local time derivatives are determined by (41) and (42). This sort of explicit time integration requires a moderately small time step size and has a clear advantage: with known displacements u_x at $x = 0, L$ we have a fixed material volume for the end of the time step, which allows finding the equilibrium by seeking $\arg\min U_\Sigma$. In practice, updating the nodal variables according to the incremental boundary conditions (45) requires a derivative of the velocity profile $v'_{\text{exit}}(y)$ as the nodal unknowns comprise not only displacements, but also their derivatives in the transverse direction.

(ii) As soon as the kinematic constraints are applied for some of the degrees of freedom of the nodes at the left and right boundaries of the domain, we proceed to the quasi-Newton iterative scheme and seek the values of the rest of degrees of freedom in the model by minimizing the total strain energy (30). At each iteration, we compute the force vector of derivatives $\partial U_\Sigma / \partial e$, and the stiffness matrix is evaluated only when the rate of convergence at the previous iteration was unsatisfactory. Converged iterations provide us with the new equilibrium state $\boldsymbol{u}^{(k+1)}$.

7 Simulation of a moving plate

We considered a plate with the width w, length L, and material properties as in the benchmark test (37). As the behavior of the system depends strongly on the ratio between the membrane and the bending stiffness of the plate, we considered two values of its thickness and started with a moderately thick plate with $h = 0.02$ (which is yet small enough compared to the dimensions w and L for the employed classical theory). The velocities at the boundaries were chosen as follows:

$$v_{\text{entry}} = 5, \quad v_{\text{exit}} = 5 + 1y. \tag{46}$$

Note that the mean value of the exit velocity varies when the line of contact is moving in the transverse direction. Thus, the linear component in v_{exit} rotates the cross-section of the plate at $x = L$ clockwise, which "pushes" the line of contact in the positive direction of the y-axis: its mean transverse displacement

$$u_y^* = \frac{1}{w}\int_{-w/2}^{w/2} u_y\big|_{\tilde{x}=L}\, \mathrm{d}\tilde{y} \tag{47}$$

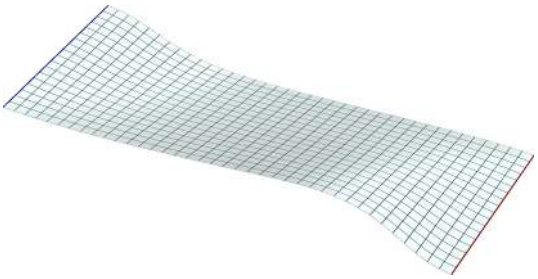

Fig. 6 Deformed configuration of the thick plate at $t = 0.4$ computed with 18 finite elements in the transverse direction

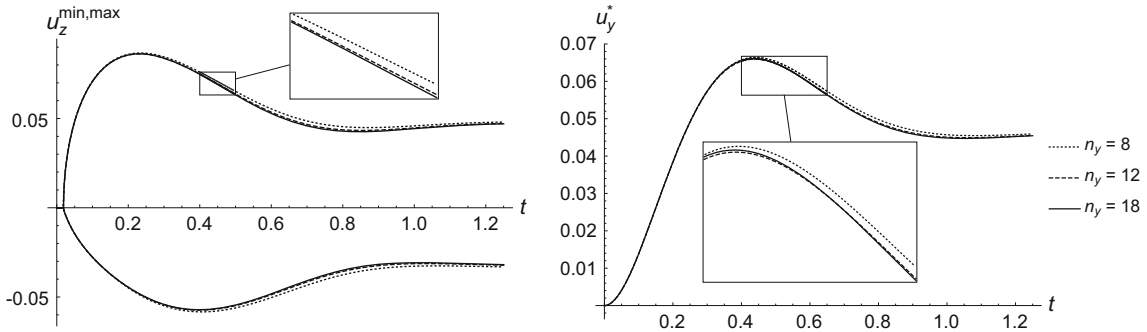

Fig. 7 Time histories of the maximal and minimal out-of-plane displacements u_z and the mean transverse displacement of the right edge u_y^* of the thick plate, computed with sequentially refined finite element models

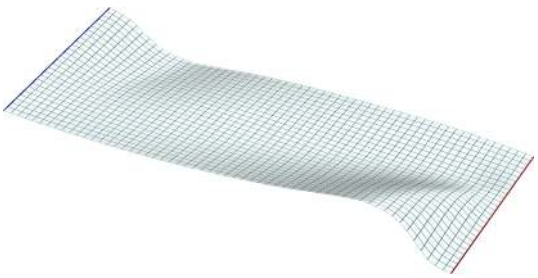

Fig. 8 Thin plate at $t = 0.4$ computed with 27 finite elements in the transverse direction, the "folds" are observable in the deformation pattern

grows in time. The mean value of v_{exit} increases as well, and a tension force appears in the plate. However, the part of the plate near $\tilde{y} = -w/2$ is compressed in the axial direction, which (along with the shear deformation owing to the motion of the line of contact) may result in the instability of the plane configuration.

We integrated over the time span $0 \le t \le 1.25$ with the step size $\tau = 0.00125$, which allowed avoiding instability in the explicit time integration of the boundary conditions for finer meshes. Experiments showed that further reduction of the time step size results in nearly identical solutions. Varying the number of finite elements in the transverse direction n_y, we kept the length to width aspect ratio of the elements $(L/n_x)/(w/n_y) \approx 1.2$.

The computed configuration of the plate at $t = 0.4$ with $n_y = 18$ is shown in Fig. 6. As discussed after (46), the linear component in v_{exit} leads to a growing in-plane deformation, which soon initiates the out-of-plane buckling of the plate. The computed time histories of the maximal and the minimal (negative) displacements u_z as well as of the mean transverse displacement of the line of contact u_y^* are shown in Fig. 7 for three levels of mesh refinement. Besides rapid mesh convergence and transition to a stationary regime, we clearly observe the time instant of buckling of the plate, at which in-plane equilibria with $u_z = 0$ become unstable and non-zero values of $u_z^{\min}$, $u_z^{\max}$ are produced in the simulation.

A thin plate with $h = 0.01$ has significantly lower bending stiffness in comparison to the membrane one, which makes the simulation more challenging from the numerical point of view. The deformed surface, presented in Fig. 8, is less smooth than the previous one in Fig. 6. Lines with high curvature ("folds") may now be observed, which require dense finite element meshes to be accurately resolved. In particular, the boundary layer

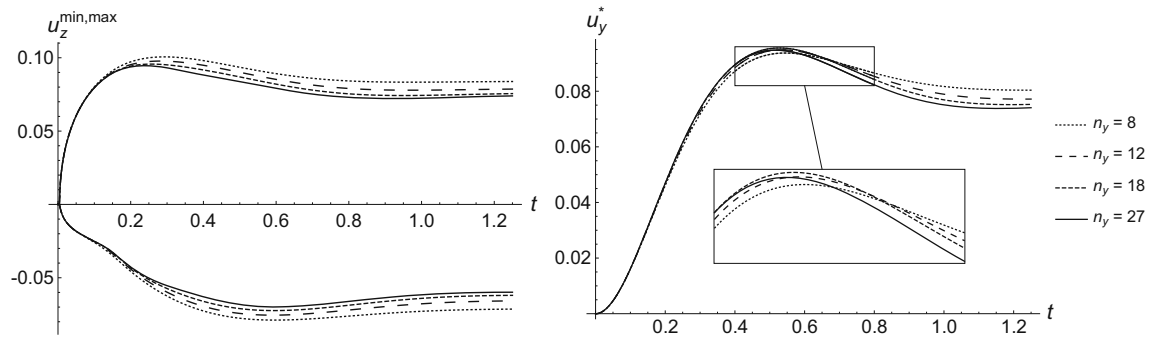

Fig. 9 Time histories of the maximal and minimal out-of-plane displacements u_z and the mean transverse displacement of the right edge u_y^* of the thin plate

near $x = L$ tends to demonstrate a complicated deformation pattern. The effect is getting more pronounced for yet thinner plates (as the one considered in the benchmark test in Sect. 5). Nevertheless, the solution with $n_y = 27$ finite elements in the transverse direction is quite accurate, as it may be concluded from the time histories, shown in Fig. 9. Earlier buckling of the thin plate may also be observed.

8 Conclusions and outlook

Consistent modeling of nonlinear deformations of axially moving plates is a challenging task, which requires both theoretical analysis as well as appropriate numerical schemes. The idea of the presented approach lies in a kinematic description, which is particularly suitable for the considered kind of problems. Although similar methods have been previously proposed for 2D, 3D and rod structures, no examples of mixed Eulerian-Lagrangian description in the nonlinear mechanics of plates could be found in the open literature.

In this first presentation of the approach, we consider purely elastic material law and restrict the analysis to the case of constant velocity v_{entry}, with which the plate is entering the domain. The most simple implementation of the approach features explicit time integration of the kinematic boundary conditions, which is accomplished by minimizing the total strain energy of the plate at each time step of the quasistatic simulation. Currently, an extension of the method toward non-homogeneous velocity profiles v_{entry} is on the way. The idea lies in the use of intrinsic strains, which are imposed in the reference configuration such that it is getting pre-stressed. Consistency of the nonlinear model is achieved by the use of multiplicative decomposition of the total tensor of deformation gradient from the incompatible undeformed configuration to the actual one via the reference and intermediate states. This and further extensions of the method will be presented in subsequent publications.

Acknowledgments Open access funding is provided by TU Wien (TUW). This work has been partially carried out at LCM GmbH as part of a K2 project. K2 projects are financed using funding from the Austrian COMET-K2 programme. The COMET K2 projects at LCM are supported by the Austrian Federal Government, the Federal State of Upper Austria, the Johannes Kepler University and all of the scientific partners which form part of the K2-COMET Consortium.

References

1. Vetyukov, Y., Gruber, P.G., Krommer, M.: Modeling finite deformations of an axially moving elastic plate with a mixed Eulerian–Lagrangian kinematic description. In: Kleiber, M., et al. (eds.) Proceedings of PCM-CMM-2015—3rd Polish Congress of Mechanics and 21st Computer Methods in Mechanics, vol. 1 (2015)
2. Chen, L.-Q.: Analysis and control of transverse vibrations of axially moving strings. ASME Appl. Mech. Rev. **58**, 91–116 (2005)
3. Humer, A., Irschik, H.: Large deformation and stability of an extensible elastica with an unknown length. Int. J. Solids Struct. **48**, 1301–1310 (2011)
4. Eliseev, V., Vetyukov, Y.: Effects of deformation in the dynamics of belt drive. Acta Mech. **223**, 1657–1667 (2012)

5. Pechstein, A., Gerstmayr, J.: A Lagrange–Eulerian formulation of an axially moving beam based on the absolute nodal coordinate formulation. Multibody Syst. Dyn. **30**, 343–358 (2013)
6. Irschik, H., Holl, H.: Lagrange's equations for open systems, derived via the method of fictitious particles, and written in the Lagrange description of continuum mechanics. Acta Mech. **226**, 63–79 (2015)
7. Ghayesh, M.H., Amabili, M., Païdoussis, M.P.: Nonlinear dynamics of axially moving plates. J. Sound Vib. **332**, 391–406 (2013)
8. Banichuk, N., Jeronen, J., Neittaanmäki, P., Tuovinen, T.: On the instability of an axially moving elastic plate. Int. J. Solids Struct. **47**, 91–99 (2010)
9. Moës, N., Dolbow, J., Belytschko, T.: A finite element method for crack growth without remeshing. Int. J. Numer Methods Eng. **46**, 1278–1300 (1999)
10. De Lorenzis, L., Temizer, I., Wriggers, P., Zavarise, G.: A large deformation frictional contact formulation using NURBS-based isogeometric analysis. Int. J. Numer. Methods Eng. **87**, 1278–1300 (2011)
11. Boman, R., Ponthot, J.-P.: Efficient ALE mesh management for 3D quasi-Eulerian problems. Int. J. Numer. Methods Eng. **92**, 857–890 (2012)
12. Donea, J., Huerta, A., Ponthot, J.-P., Rodriguez-Ferran, A.: Arbitrary Lagrangian–Eulerian methods. In: Stein, E., de Borst, R., Hughes, T.J.R. (eds.) Encyclopedia of Computational Mechanics Volume 1: Fundamentals, Chapter 14. Wiley, Amsterdam (2004)
13. Kainz, A.J., Widder, M.E., Zeman, K.: Enhanced strip-roll coupling concepts for the numerical simulation of flat hot rolling. Acta Mech. **224**, 957–983 (2013)
14. Ciarlet, P.G.: An introduction to differential geometry with applications to elasticity. J. Elast. **1–3**, 1–215 (2005)
15. Opoka, S., Pietraszkiewicz, W.: On modified displacement version of the non-linear theory of thin shells. Int. J. Solids Struct. **46**, 3103–3110 (2009)
16. Eliseev, V.V.: Mechanics of Deformable Solid Bodies (in Russian). St. Petersburg State Polytechnical University Publishing House, St. Petersburg (2006)
17. Eliseev, V.V., Vetyukov, Y.: Finite deformation of thin shells in the context of analytical mechanics of material surfaces. Acta Mech. **209**, 43–57 (2010)
18. Vetyukov, Y.: Finite element modeling of Kirchhoff–Love shells as smooth material surfaces. ZAMM **94**, 150–163 (2014)
19. Altenbach, J., Altenbach, H., Eremeyev, V.A.: On generalized Cosserat-type theories of plates and shells: a short review and bibliography. Arch. Appl. Mech. **80**, 73–92 (2010)
20. Vetyukov, Y.: Nonlinear mechanics of thin-walled structures: asymptotics, direct approach and numerical analysis. Springer, Vienna (2014)
21. Stoker, J.J.: Differential Geometry. Wiley, Amsterdam (1989)